

Supporting Information:

Photothermal Circular Dichroism of Single Nanoparticles Rejecting Linear Dichroism by Dual Modulation

Patrick Spaeth,^{†,‡} Subhasis Adhikari,^{†,‡} Martin Dieter Baaske,[†] Sergii Pud,[†]
Jacco Ton,[†] and Michel Orrit^{*,†}

[†]*Huygens Kamerlingh Onnes Laboratory, Leiden University, 2300 RA Leiden, Netherlands*

[‡]*These authors contributed equally*

E-mail: orrit@physics.leidenuniv.nl

Stokes representation of polarization

The Stokes parameters of polarized light are usually employed when describing partially polarized light and thus allow for a more general treatment than the Jones calculus representation of polarization. Here, even though we only deal with fully polarized light, we still introduce the Stokes definition of polarization as it provides a convenient expression of

polarization states in terms of the four Stokes parameters, which are defined as

$$S_0 = \langle E_x^2 + E_y^2 \rangle$$

$$S_1 = \langle E_x^2 - E_y^2 \rangle / S_0$$

$$S_2 = \langle E_x E_y \cos(\delta) \rangle / S_0$$

$$S_3 = \langle E_x E_y \sin(\delta) \rangle / S_0$$

E_x and E_y are the respective x and y components of the electric field and δ is the phase difference of the two components. With this definition we have

- horizontal polarization if $S_1 = 1$
- vertical polarization if $S_1 = -1$
- linear 45° polarization if $S_2 = 1$
- linear -45° polarization if $S_2 = -1$
- right circular polarization if $S_3 = 1$
- left circular polarization if $S_3 = -1$

Experimental alignment procedure

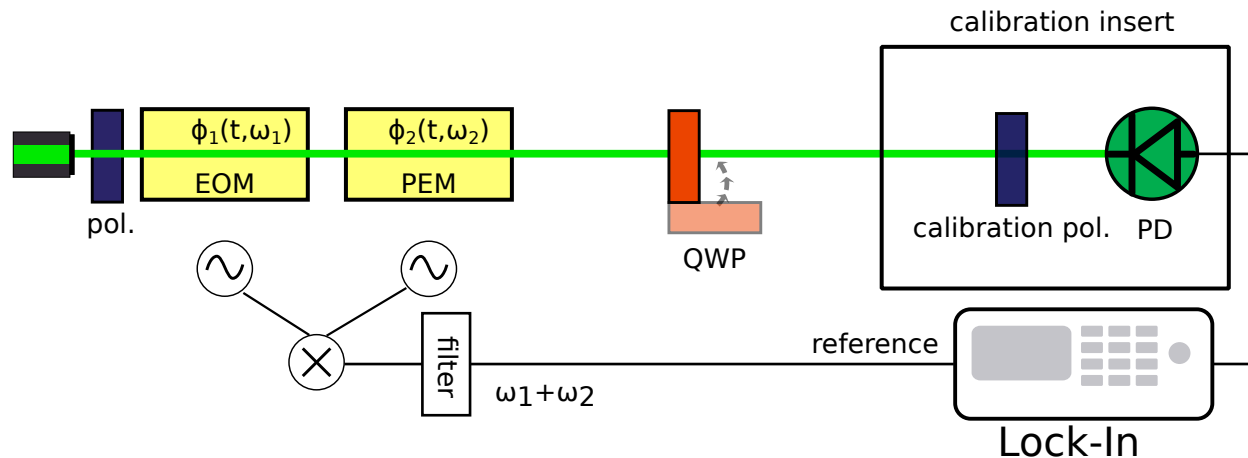


Figure S1: Heating arm of the dual modulation setup. The polarization modulation is performed by an EOM and a PEM, followed by a set of static retarders (QWP, CB_{45} and CB_{90}). A calibration unit composed of a rotatable polarizer and a fast photodiode is inserted for alignment of the polarization modulation. The configuration illustrated here, with the QWP inserted, corresponds to the mode sensitive to circular dichroism (CD-sensitive).

In this section we will give a description of the alignment procedure of the heating arm of our dual-modulation setup. The heating part of the setup, the one that is polarization-modulated, is illustrated in Figure S1. It consists of two polarization modulators, an EOM and a PEM. A set of static birefringent elements, QWP, CB_{45} and CB_{90} changes the measurement mode of the setup and allows us to measure different absorptive properties, as explained in the main text. After the birefringent plates we add a calibration unit consisting of a rotatable polarizer and a fast photodiode. The photodiode's output is sent to a lock-in amplifier which is referenced to the sum frequency of the two modulators.

The purpose of the alignment procedure is to make the setup sensitive to one of the following absorptive properties, isotropic absorption, linear dichroism (LD), and circular dichroism (CD), while as much as possible reducing cross-talk between these properties. Plasmonic nanoparticles can in principle exhibit both linear dichroic and circular dichroic behaviour. In samples consisting of plasmonic nanoparticles, the linear dichroism is often much larger than the respective circular dichroism. When we aim to measure the CD of such

particles, we should therefore take great care to avoid any leakage of the much stronger LD into the weak CD signal.

In our previous report of photothermal circular dichroism^{S1} we used a single, square-modulation scheme of the polarization, performed by an EOM. We aimed to modulate between purely left and purely right circular polarization. In principle, a square-wave modulation of the polarization is an ideal scheme to measure circular dichroism, as it completely avoids linear polarization states. However, this scheme requires a virtually perfect square-wave modulation of the polarization. This is practically not feasible when performing the modulation at high frequencies (10 kHz), in particular due to bandwidth limitations of the electronics and piezoelectric behaviour of the EOM crystal. Any imperfection of the square-wave pattern can lead to a cross talk of LD and CD, thereby creating artefact signals. Secondly, the EOM, on top of the polarization modulation, also performs a slight modulation of the intensity. This effect is called residual amplitude modulation^{S2} and it will induce an artefact signal for any absorbing particle.

To avoid both effects, the cross talk between LD and CD as well as the RAM, we exploited past developments in the field of CD spectroscopy,^{S3-S5} where two or more polarization modulators are used simultaneously to analyze different combinations of the driving frequencies of the two modulators, thereby giving access to various sample properties. We perform lock-in detection and thus only measure at a single frequency. But we still benefit of the two-modulator scheme if we perform our measurement at the sum (or difference) frequency of the two modulators. We will describe in section 2 how to measure different absorptive properties at the sum frequency of the two modulators by using different static retarders placed after the modulators. At the sum frequency the modulators' individual residual amplitude modulation is of second order in these small effects, and can be neglected. In the following we will describe an alignment procedure that solves the problem of cross talk between LD and CD. Here we also benefit from the two-modulator scheme as it provides additional tuning parameters that allow us to remove cross talk better.

We concluded from our previous measurements,^{S1} that a perfect square-wave modulation of the polarization by the EOM is not feasible and therefore we use a sinusoidal modulation of the polarization. Because of its mechanical resonance, the PEM only provides sinusoidal modulation. In both cases, the retardance created by each individual modulator varies sinusoidally with time and thereby not only creates circular but also elliptical and linear polarization states. One might think that this would inevitably cause cross talk between LD and CD. However, when we choose suitable modulation parameters and perform a thorough alignment of the components we can probe all absorptive properties of a sample with negligible cross talk between them. As illustrated in Figure S1 the dual modulation of the polarization is performed using an EOM and a PEM. The laser beam first passes the EOM, then the PEM. We found that this arrangement of the two modulators is convenient for the rejection of LD induced artefacts, because the static birefringence of the EOM can be more easily adjusted to compensate for imperfections of the polarization optics.

Alignment protocol

The alignment procedure we developed is composed of two steps. In the first step we align the fast axes of all components and make their optical axes collinear with the beam propagation. As the EOM contains a thick uniaxial crystal we must carefully align its crystal axis along the laser beam. In the first alignment step we make sure that the setup gives a CD response with the proper polarization optics. The second step is dedicated to ensure a pure CD measurement of the setup, free from cross talk. Later, we will also discuss how to probe other absorptive properties. The protocol that we developed is as follows:

First we make sure that we have a well-defined and clean linear polarization state. To this purpose, we use a Glan-Thomson polarizer (extinction ratio 10^{-5}) oriented such that we have horizontally polarized light, or in terms of Stokes parameters: $S_1 = 1$. To measure the polarization state we use a Schaefer & Kirchhoff polarization analyzer, which conveniently displays the polarization state in terms of the Stokes parameters. After the polarizer we send

the laser beam through the EOM. For the rough alignment procedure the time-dependent retardation of both modulators is turned off.

EOM alignment: We first roughly align the EOM fast axis to 45° with respect to the initial polarization. Then we align the EOM's optical axis along the propagation direction according to the alignment procedure described in.^{S6} Finally we align the EOM's fast axis precisely at 45° with respect to the initial polarization. Assuming that we have purely horizontal linearly polarized light $S_1= 1$ and $S_2= 0$, if the EOM's fast axis was aligned perfectly at 45° with respect to the initial polarization, when applying a retardation along the fast axis we would not create an S_2 component but only a S_3 component of the polarization. To align the fast axis we thus measure the polarization state while applying a large static retardation and rotate the EOM along its crystal axis, until the S_2 component vanishes.

PEM alignment: The alignment of the PEM is simpler, for it consists of fused silica instead of a uniaxial crystal, thus there is no crystal axis the beam needs to be aligned to. However, the path length of the beam through the crystal defines the phase retardation and therefore we make sure we align the surface normal of the silica plate with the propagation axis of the laser beam. The retardation amplitude of the PEM is also slightly dependent on the position where the laser beam impinges on the quartz plate. To make sure that we exert the desired retardation amplitude we manually place the PEM such that we hit the center of the quartz plate. The PEM fast axis alignment is performed similar to the EOM fast axis alignment, but while applying a dynamic retardation instead.

Alignment of QWP: After the PEM, the laser beam passes through a number of static linear and circularly birefringent components that allow us to set the operation mode of the setup. To be sensitive to CD, the differential absorption of left and right circularly polarized light, we need to insert a QWP after the two modulators. The achromatic QWP (Thorlabs) is mounted in a rotational optical mount to ensure precise alignment of the fast axis. To align it we measure the polarization state after the QWP while rotating the fast axis so that the polarization state is purely circular, $| S_3 | = 1$.

Alignment of CB plates: The setup contains two circular birefringent components that can change the measurement mode in case we want to measure LD. Both of them are circularly birefringent plates, made from crystalline α -quartz, with a rotatory strength of either 45° or 90° (at 532 nm). We will later come back to explain the purpose of these plates, for now we only explain their alignment. A purely circularly birefringent component does not possess a fast axis, but the path length of the laser beam through the component defines the rotatory strength of the plate. The path length can be adjusted by tilting the surface normal of the plate with respect to the propagation direction of the laser beam. We first measure the polarization state before we insert the plates. Assuming a perfect horizontal polarization, $S_1 = 1$, before the circular birefringent plates, we get $S_2 = -1$ for the CB₄₅ plate and $S_1 = -1$ for the CB₉₀ plate.

The procedure that we discussed so far was the rough alignment procedure. If we chose suitable combinations of the static retarding elements we would already be able to measure different properties of an absorbing sample. However, these measurements might not be free from cross talk between LD and CD. A second step of alignment is required to make it exclusively sensitive to a single absorptive property, meaning that we suppress the cross talk between LD and CD. Up to now, the time-dependent retardation of the polarization modulators was turned off. For this second step, both modulators are set to perform a non-biased sinusoidal modulation with a retardation amplitude of $\pi/2$, the EOM at frequency ω_1 and the PEM at frequency ω_2 . We insert a photodiode and a rotatable polarizer (calibration polarizer), as illustrated in Figure S1. The polarizer represents a purely linear dichroic element. The photodiode is connected to a lock-in amplifier, which is referenced to the sum frequency of the two modulators. We bring the setup to the CD-sensitive mode, which corresponds to the configuration with two modulators plus the QWP. As we modulate the polarization with both modulators, the intensity transmitted through the calibration polarizer changes as a function of time. The lock-in compares the intensity transmitted through the polarizer with the external reference ($\omega_1 + \omega_2$) while extracting modulations occurring only at this

very frequency. We shall thus call the part of the transmitted intensity that is modulated at frequency $\omega_1 + \omega_2$ our signal.

If we are in CD-sensitive mode, no signal is expected when the calibration polarizer is inserted, as it is only linearly but not circularly dichroic. However, due to slight imperfections in the modulation scheme, such as misalignment of the fast axes of the EOM, PEM or QWP, bias retardation of the modulators, or deviation of the QWP's retardation strength, we have to anticipate a nonzero cross talk of LD and CD and therefore also a signal. The strength of the signal measured by the lock-in, while the polarizer is inserted, is a measure of the cross talk between LD and CD. We found that we can compensate the aforementioned imperfections of the components and the alignment, thereby we reduce the cross talk. To achieve this it is sufficient to adjust two parameters, the EOM bias retardation and the QWP's fast axis.

Fine alignment procedure:

First we rotate the calibration polarizer such that it transmits $S_1 = 1$ and we minimize the lock-in signal at the sum frequency by adjusting the EOM's bias retardation. Then we rotate the calibration polarizer to transmit $S_2 = 1$ and minimize the signal by adjusting the fast axis of the QWP. To understand this second alignment procedure it is important to have a closer look at LD. Linear dichroism which is defined as the differential absorption of two orthogonal polarization states is, unlike CD, dependent on the in-plane orientation of the object under study. To retrieve the full linear dichroic behaviour of an object, two measurements are necessary, one where we probe the absorption difference of $S_1=1$ and $S_1=-1$, which we shall call LD_{\perp} , and one where we probe the absorption difference of $S_2 =1$ and $S_2=-1$, and which we call LD_{\sphericalangle} . When we try to avoid cross talk of LD and CD we need to make sure to avoid cross talk of both LD_{\perp} with CD and LD_{\sphericalangle} with CD. We found that the change of the EOM bias retardation affects exclusively the cross talk between LD_{\sphericalangle} and CD, while the rotation of the QWP's fast axis affects exclusively the cross talk between LD_{\perp} and CD, at least within a reasonable range. This behaviour is represented in Figure 2 of the main text.

Quantification of the extinction ratio

With the calibration insert, shown in Figure S1, which is composed of the rotatable polarizer and the photodiode, we can not only tune the setup for reducing the cross talk, but we are also able to quantify this cross talk. This is especially important when measuring particles that have strong LD compared to their CD, such as plasmonic nanorods, or plasmonically coupled metal nanospheres.^{S7-S9} Although we achieve very high rejection of cross talk we are not able to completely eliminate it. To quantify the residual cross talk we define a rejection ratio, that tells by which factor we suppress the leakage of LD into CD. The experimental extinction ratio is defined as:

$$R_{ext}(\alpha) = \frac{LD_{pol}}{CD_{pol}}. \quad (1)$$

To determine the rejection ratio we need to measure the two quantities CD_{pol} & LD_{pol} . Therefore we first put the setup in LD_{\sphericalangle} -sensitive mode and rotate the calibration polarizer to maximize the lock-in signal. The obtained maximum value is LD_{pol} . Then we switch to CD-sensitive mode by inserting the QWP and again measure the lock-in signal. The obtained value is CD_{pol} . CD_{pol} is in general dependent on the angle of the polarizer. This indicates that there is a different amount of cross talk from LD_{\sphericalangle} into CD, and from LD_{\perp} into CD. We typically measure a rejection of 200 at polarizer positions of $n \cdot 90^{\circ}$. For polarizer positions of $45^{\circ} + n \cdot 90^{\circ}$ we measure a rejection ratio of 6×10^4 . For our measurements we assume the worst case corresponding to the lowest rejection ratio, 200. We want to note here that this rejection ratio is mutual. If we suppress the LD leakage into CD we also suppress the leakage of CD into LD.

In case we seek to have even stronger rejection of cross talk we make use of the aforementioned CB_{90} plate as described in.^{S4} The CB_{90} plate rotates all linear polarization states by 90° regardless of their orientation. This effectively flips the sign of LD, while maintaining its magnitude. On the other hand, as the CB_{90} plate does not affect circular polarization

states, the circular dichroism measurement is not affected. Thus, in order to even further reduce the cross talk, we can perform two circular dichroism measurements, one with and one without the CB_{90} plate. If we then average these two measurements we remove the residual LD contribution.

Simulations

In a dual polarization modulation scheme, the time-dependent power absorbed by a sample can be composed of many different combinations of the frequencies driving the two modulators, ω_1 and ω_2 , depending on the properties of the sample under study. In this section we want to simulate the time-dependent power absorbed by a given sample using Jones matrix calculus. We then extract the frequency spectrum by applying a FFT of the absorbed power. In principle one could also perform an analytical calculation of the frequency decomposition of an arbitrary sample as presented in.^{S5} However, our numerical approach allows us to conveniently explore a large space of parameters, which would be tedious to calculate with an analytical approach.

Jones matrix representation of the optical components

The matrix formalism developed by Jones^{S10-S16} provides a convenient framework for analyzing the effects of optical components on fully polarized light. The matrix representations for the different optical components were taken from refs.^{S10,S13,S16}

Rotation Matrix:

$$\mathbf{R}_\Theta := \begin{bmatrix} \cos(\Theta) & \sin(\Theta) \\ -\sin(\Theta) & \cos(\Theta) \end{bmatrix}, \quad (2)$$

With the rotation matrix \mathbf{R}_Θ it is possible to calculate the matrix representation of axially rotated elements. Assuming that the optical component has a matrix representation of \mathbf{M} in a certain reference frame, when the component is rotated by an angle Θ in clockwise sense, then the matrix of the rotated element can be expressed as $\mathbf{M}_\Theta = \mathbf{R}(-\Theta)\mathbf{M}\mathbf{R}(\Theta)$.

Linearly birefringent plate:

$$\Phi(\eta, \Theta) := \mathbf{R}(-\Theta) \begin{bmatrix} 1 & 0 \\ 0 & e^{i\eta} \end{bmatrix} \mathbf{R}(\Theta). \quad (3)$$

In the simplest case of a static birefringent plate, η is a constant value. We can model a polarization modulator with a time-dependent retardance as $\eta(t) = \eta_0 \sin(\omega t) + \phi_0$, where η_0 is the retardation amplitude, ω the modulation frequency and ϕ_0 an additional static linear birefringence.

Circularly birefringent plate:

$$\mathbf{CB}_\alpha := \begin{bmatrix} \cos(\alpha) & \sin(\alpha) \\ -\sin(\alpha) & \cos(\alpha) \end{bmatrix}, \quad (4)$$

with α being the rotatory strength (optical activity) of the CB plate.

With the above defined Jones matrices and for horizontally polarized light as input, we can write the time-dependent electric field of the polarization modulator setup that is illustrated in Figure S1 as

$$\begin{bmatrix} E_{x0} \\ E_{y0} \end{bmatrix} (t) = \mathbf{CB}_\alpha \Phi_0(\eta_0, \Theta_0) \Phi_2(\eta_2, \Theta_2, \omega_2, t) \Phi_1(\eta_1, \Theta_1, \omega_1, t) \begin{bmatrix} 1 \\ 0 \end{bmatrix}, \quad (5)$$

where $\Phi_{1,2}$ represent the matrices of the polarization modulators and Φ_0 a static linear retarder (QWP).

Often, the Jones matrix approach is used to calculate the light transmitted through a sample. This approach represents the CD measurements performed with commercial CD spectrometers well, as they measure the transmission of a dilute solution of molecules in a cuvette. The measurements that we perform, however, are true absorption measurements

and therefore require a different matrix representation of the samples in terms of absorption. This representation has been described by Jones in.^{S16} The different absorptive properties of a sample can be modeled as follows:

Isotropic absorber:

$$\mathbf{u} := -\kappa \begin{bmatrix} u & 0 \\ 0 & u \end{bmatrix} \quad (6)$$

with κ being the amplitude absorption coefficient.

LD_⊥ absorber:

$$\mathbf{ld}_{\perp} := \mathbf{p}_{\perp} \begin{bmatrix} 1 & 0 \\ 0 & -1 \end{bmatrix} \quad (7)$$

with \mathbf{p}_{\perp} being half the difference of the two principal absorption coefficients.

LD_∠ absorber:

$$\mathbf{ld}_{\angle} := \mathbf{p}_{\angle} \begin{bmatrix} 0 & 1 \\ 1 & 0 \end{bmatrix} \quad (8)$$

with \mathbf{p}_{\angle} being half the difference of the two principal absorption coefficients.

CD absorber:

$$\mathbf{cd} := \delta \begin{bmatrix} 0 & -i \\ i & 0 \end{bmatrix} \quad (9)$$

with δ being half the difference of the absorption coefficients of left and right circular polarizations.

With the definitions for the samples given in equations 6-9 it is possible to represent an absorber exhibiting various absorptive properties by just adding the respective sample

matrices.

Assuming the particle under study behaves as a dipole, the time-averaged power absorbed by the particle can be expressed as

$$\langle \mathcal{P}_{abs} \rangle(\omega_1, \omega_2) = -\langle \text{Im}[\vec{p}^*(\omega_1, \omega_2) \cdot \vec{E}(\omega_1, \omega_2)] \rangle \quad (10)$$

with

$$\vec{p} = \vec{\alpha} \vec{E} \quad (11)$$

where \vec{p} is the dipole moment and $\vec{\alpha}$ the polarizability tensor of the absorbing dipole.^{S17} When we refer to the time average we imply time average over the optical frequencies, but not the frequencies of the polarization modulators, this is indicated by the (ω_1, ω_2) dependence. In general, when performing a transmission assay, one would measure the extinction and not the absorption, in which case one also would need to take the real part of the polarizability into account. In photothermal microscopy, as we perform a true absorption measurement, we must only take the imaginary part of the polarizability into account,^{S18} which can be expressed by linear combinations of equations 6-9.

Simulated FFT spectra of different absorbers

In our simulations we investigate the time-dependent absorbed power of samples exhibiting different absorptive properties. We first calculate the absorbed power, according to equation 10, for the four different absorptive properties defined in 6-9, and plot it in the frequency domain by applying a FFT. Figure S2 shows the frequency spectra of four absorbers exhibiting either pure CD, pure LD_{\perp} , pure LD_{\sphericalangle} or pure isotropic absorption. The spectra are calculated for the CD-sensitive setup configuration. For the differential absorptivities we choose $\delta=10^{-3}$, p_{\perp} & $p_{\sphericalangle}=5\times 10^{-2}$ and $\kappa=0.5$.

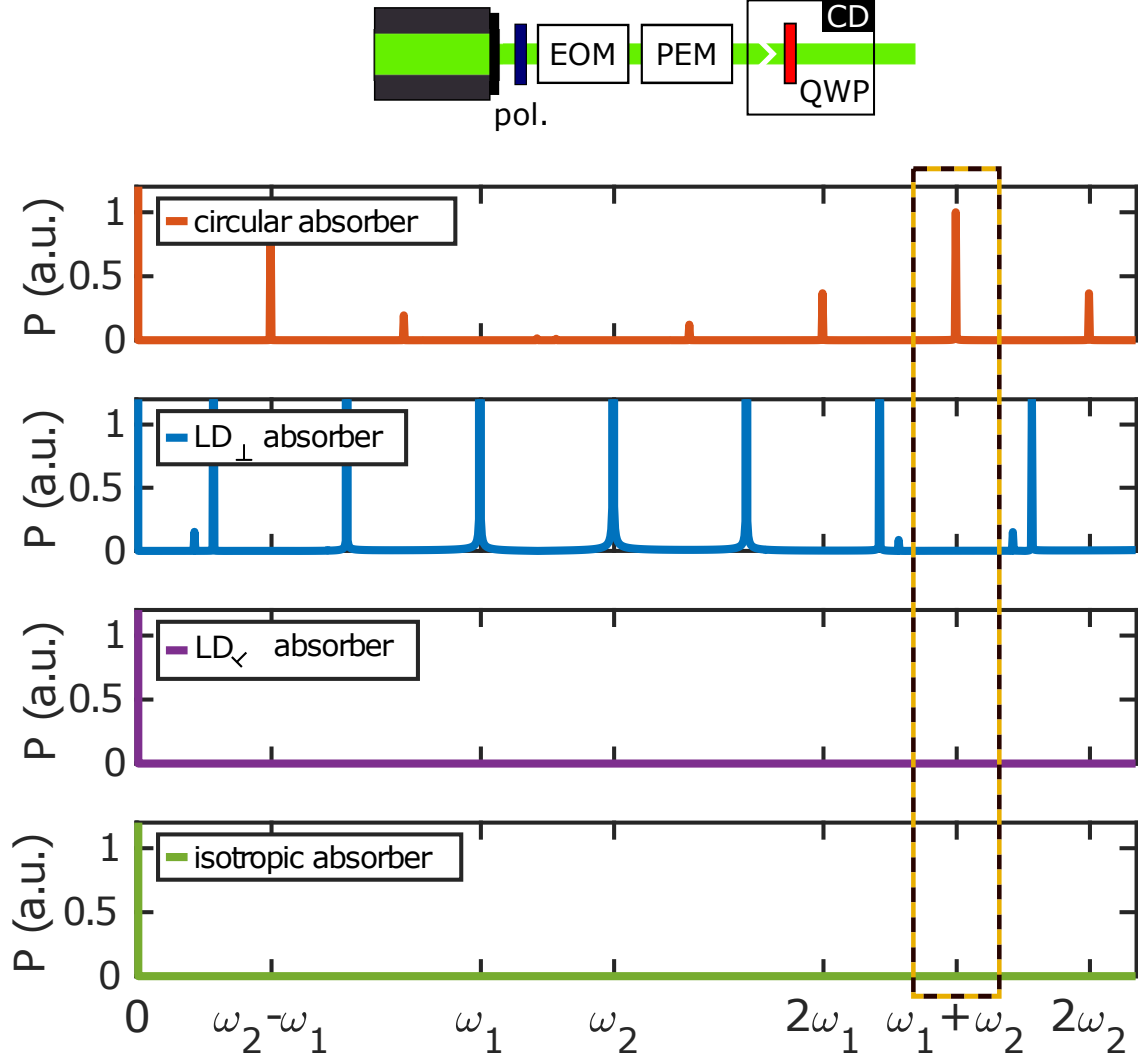


Figure S2: Spectrum of the absorbed power of the four different absorbers, exhibiting either only CD, LD $_{\perp}$, LD $_{\sphericalangle}$ or isotropic absorption, under dual polarization modulation in CD-sensitive mode. We normalize the power to 1 for the circular absorber at the sum frequency $\omega_1 + \omega_2$.

In CD mode, if we extract the signal at the sum frequency $\omega_1 + \omega_2$, we only have a contribution from the circular dichroic sample. If we want to measure the other absorptive properties at the sum frequency we have to change the mode of the setup as discussed in the alignment protocol. In our computational model this is done by modifying the components of equation 5.

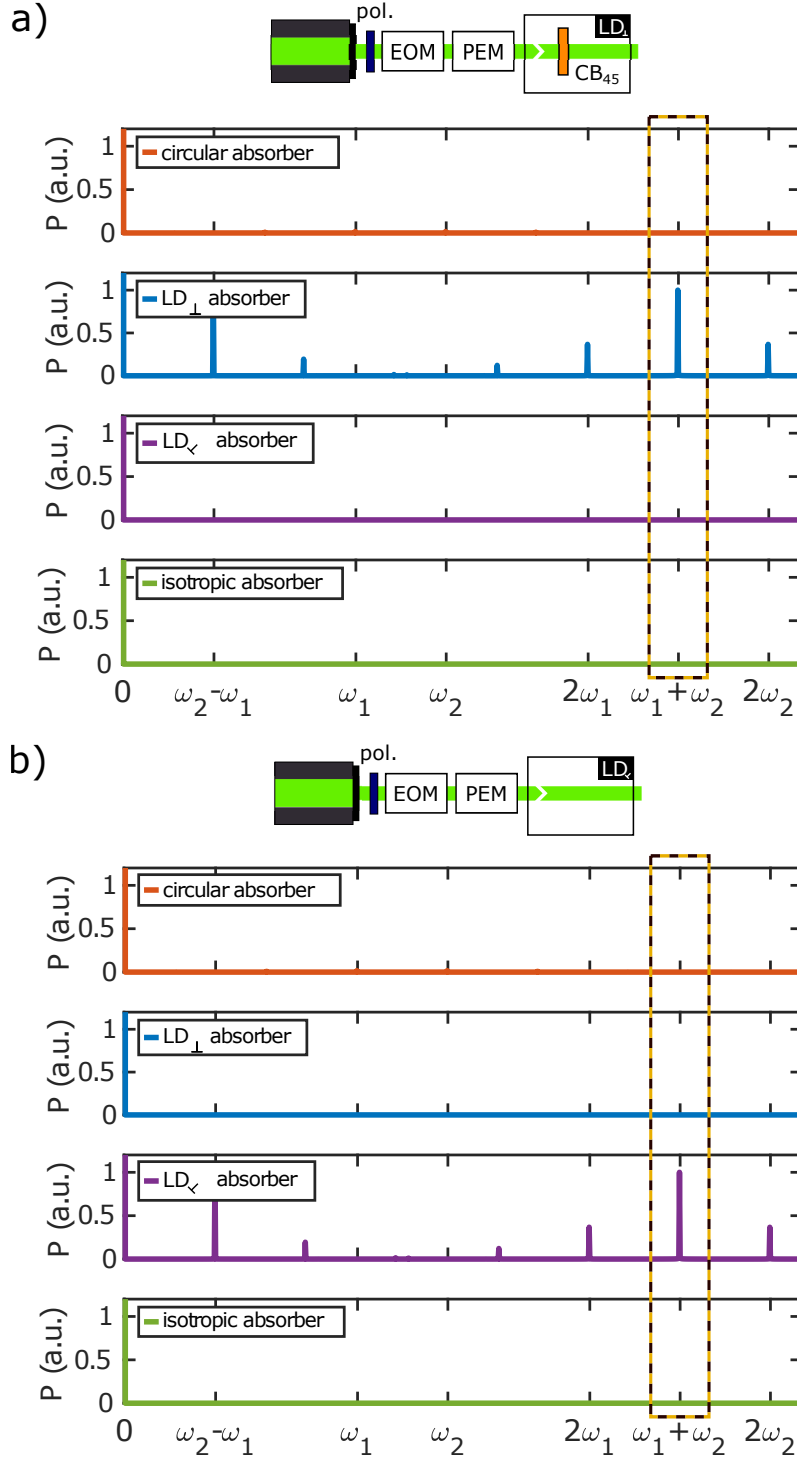


Figure S3: Spectrum of the absorbed power of the four different absorbers, exhibiting either CD, LD $_{\perp}$, LD $_{\gamma}$ or isotropic absorption, under dual polarization modulation. In a) for LD $_{\perp}$ -sensitive and b) LD $_{\gamma}$ -sensitive mode. We normalize the power to be 1 for a) the LD $_{\perp}$ absorber and for b) LD $_{\gamma}$ the absorber, at the sum frequency $\omega_1 + \omega_2$.

Figure S3a) shows the spectrum of the absorbed power of the same set of absorbers in LD_{\perp} -sensitive mode. We can indeed observe that the linear dichroic absorber LD_{\perp} has a component at $\omega_1+\omega_2$. Likewise Figure S3b) shows the power spectrum of the same set of absorbers now in the LD_{\sphericalangle} -sensitive mode. As expected only the LD_{\sphericalangle} absorber has a component at the sum frequency $\omega_1+\omega_2$. Note that in all three cases (Figure 1-2), the isotropic absorber only shows constant absorption (at $f = 0$), which is also expected as we do not perform intensity but only polarization modulation.

Until now we have only considered ideal conditions, in which we can easily ensure zero cross talk between LD and CD, and there is no artefact signal due to residual amplitude modulation. In a real setup we have to consider imperfections of the optical components themselves as well as slight misalignment of the various components. Owing to our numerical approach we can easily simulate the effect of these imperfections. These imperfections will have an effect on the spectrum of the absorbed power and introduce a cross talk between the different absorptive properties. To illustrate the influence of one particular configuration we now introduce the following set of imperfections:

- EOM residual intensity modulation of 10^{-3}
- PEM residual intensity modulation of 10^{-3}
- PEM fast axis misalignment of 0.5°
- QWP deviation of $\pi/200$ from $\pi/2$ retardation

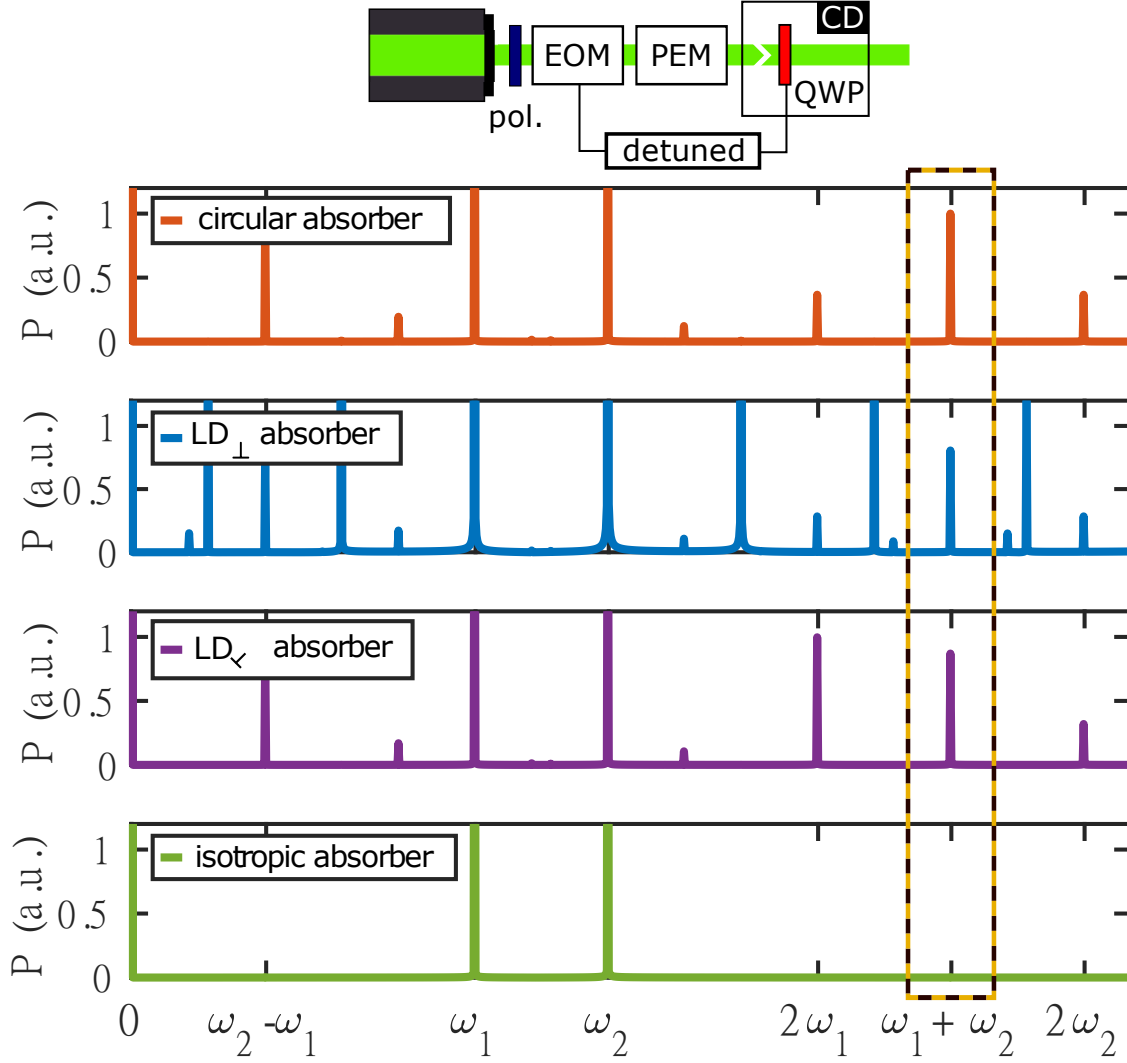


Figure S4: Spectrum of the absorbed power of the four different absorbers, under dual polarization modulation with additional imperfections of the modulation scheme, which lead to cross talk of linear and circular dichroism. We normalize the power to be 1 for the circular absorber at the sum frequency $\omega_1 + \omega_2$.

In case the g-factor of CD and LD in a sample is of the same order of magnitude, small imperfections would not have a great impact on the CD measurement. However, when investigating the CD of plasmonic nanoparticles such as nanorods, the effect of LD can be much stronger. Therefore, in our simulations, we set the CD to be a factor of 50 weaker than the LD. Figure S4 shows the power spectrum in CD-sensitive mode under the aforementioned imperfections of the polarization modulation. In this case, also the LD_{\perp} as well as the LD_{∇}

show power absorption at the sum frequency, indicating a cross talk of LD into CD. As opposed to Figures S2-S3 here the isotropic absorber shows a frequency component at ω_1 and ω_2 which is due to the slight residual intensity modulation of the polarization modulators.

The set of imperfections that we have used here is just one single example, other combinations are possible depending on the alignment and the individual components. In general there can also be more sources of imperfections induced by other optical components that we haven't discussed so far for simplicity. These can be additional optical components in the beam path. We found that with the alignment protocol described in the above sections we can compensate also for small birefringent and dichroic effects on the polarization exhibited by these additional components. The code that we used for the simulations shown here will be accessible on reasonable request.

CD of gold nanoparticle dimers

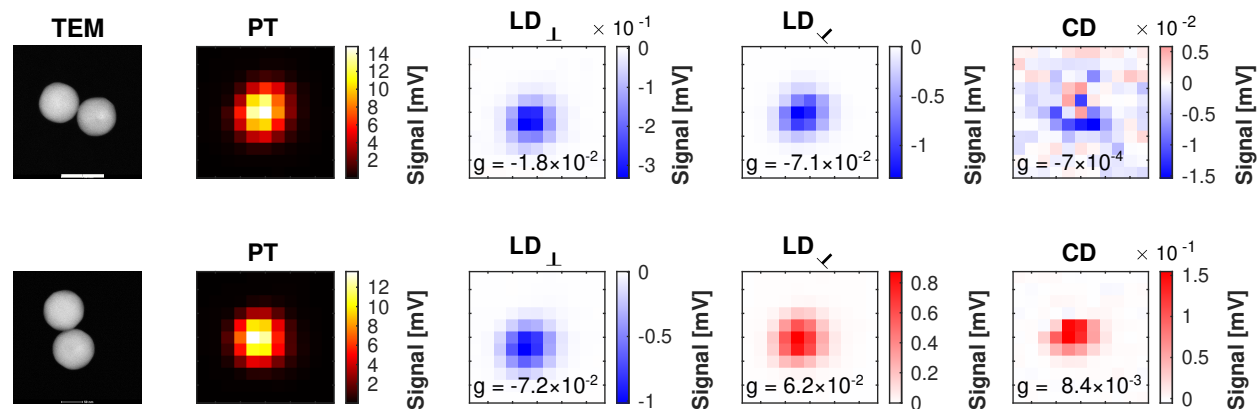


Figure S5: Correlated TEM images and optical measurements of two different 100 nm diameter gold nanoparticle dimers. One dimer is showing relatively strong PT CD signal, the other one shows weak CD signal. The measurements were performed at a heating wavelength of 532 nm. The scale bar in the TEM image is 100 nm.

Figure S5 shows correlated TEM and optical measurements of two dimer gold nanoparticles. The measurements are carried out in immersion oil as photothermal medium. One dimer exhibits relatively strong CD of 0.8%, the second particle exhibits a CD of 0.07% which is

one magnitude lower. The LD_{\perp} and LD_{\sphericalangle} are both one or two orders of magnitude larger than the CD values, which probably is induced by plasmonic hybridization.

Histogram of CD g-factors of single nanoparticles

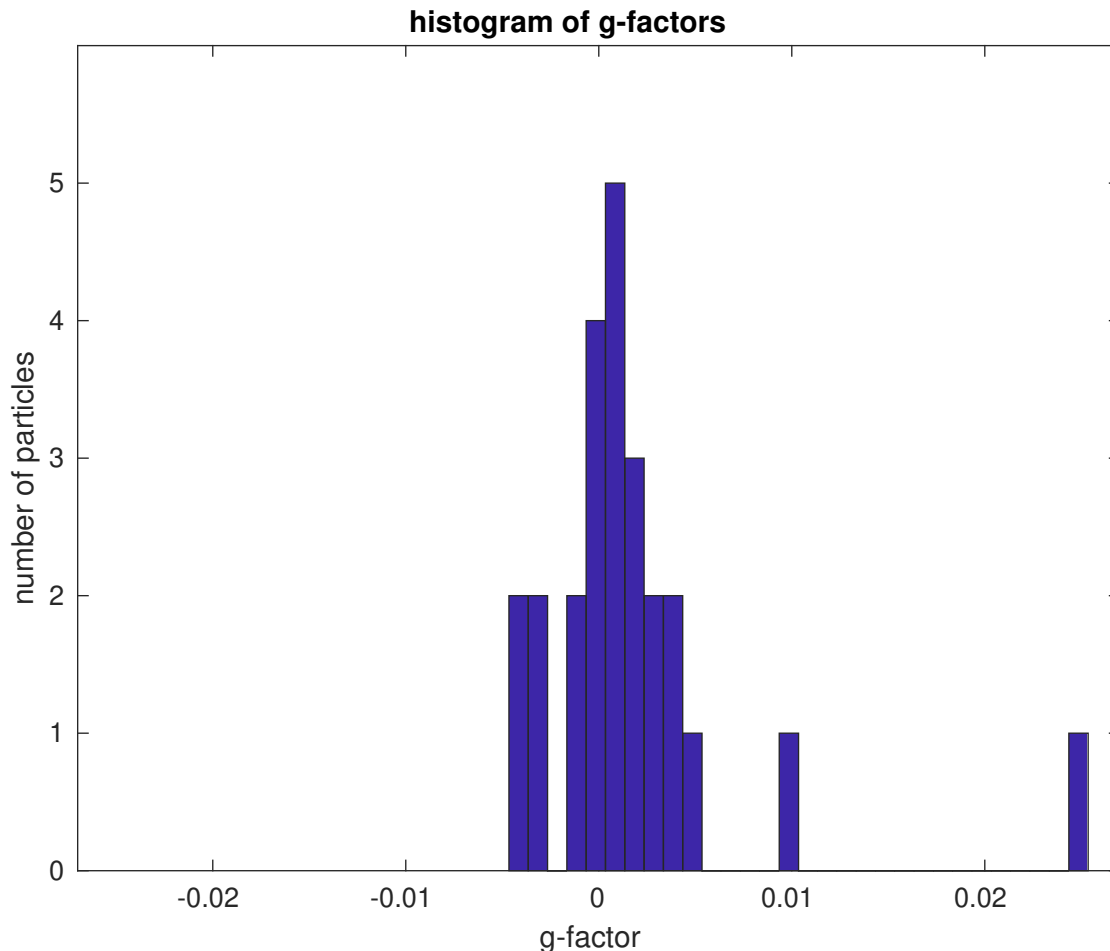


Figure S6: Histogram of g-factors of 25 single spherical gold nanoparticles. The optical measurements were carried out in immersion oil, the correlated TEM images are not shown here.

Figure S6 shows a histogram of g-factors of 25 single 100 nm diameter spherical gold nanoparticles. The mean value of g-factors is 1.7×10^{-3} which is smaller than the standard deviation of 5.8×10^{-3} . We therefore conclude that there is no CD bias for these particles.

CD of a single gold nanoparticle in carvone with LD reference

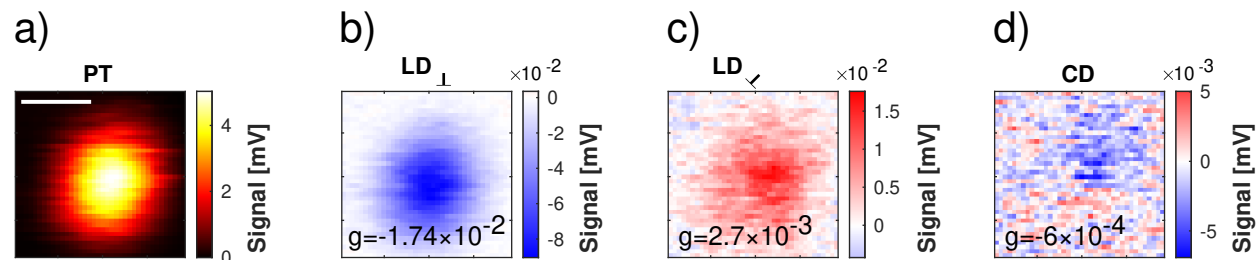


Figure S7: PT (a) LD_{\perp} (b) LD_{\parallel} (c) and CD (d) scans of the single 100 nm diameter spherical gold nanoparticle in Figure 5 of the main text. All measurements here were carried out in R-carvone. The scale bar is 250 nm. The inserts of (b)-(d) show the respective g-factors.

Figure S7 shows absorption scans of a single gold nanoparticle. The particle was chosen such that it exhibits both weak CD and weak LD, to make sure that there is no residual leakage of LD into CD and that thermal induced reshaping does not decrease the CD over the course of the experiment shown in Figure 5 in the main text. The corresponding g-factors of LD and CD are indicated in the scans. If we take into account our previously shown LD rejection ratio of 300 we expect a residual leakage of LD into CD of not larger than 5×10^{-5} in g-factor which is one magnitude lower than the particles' actual CD g-factor.

Heat-induced reshaping

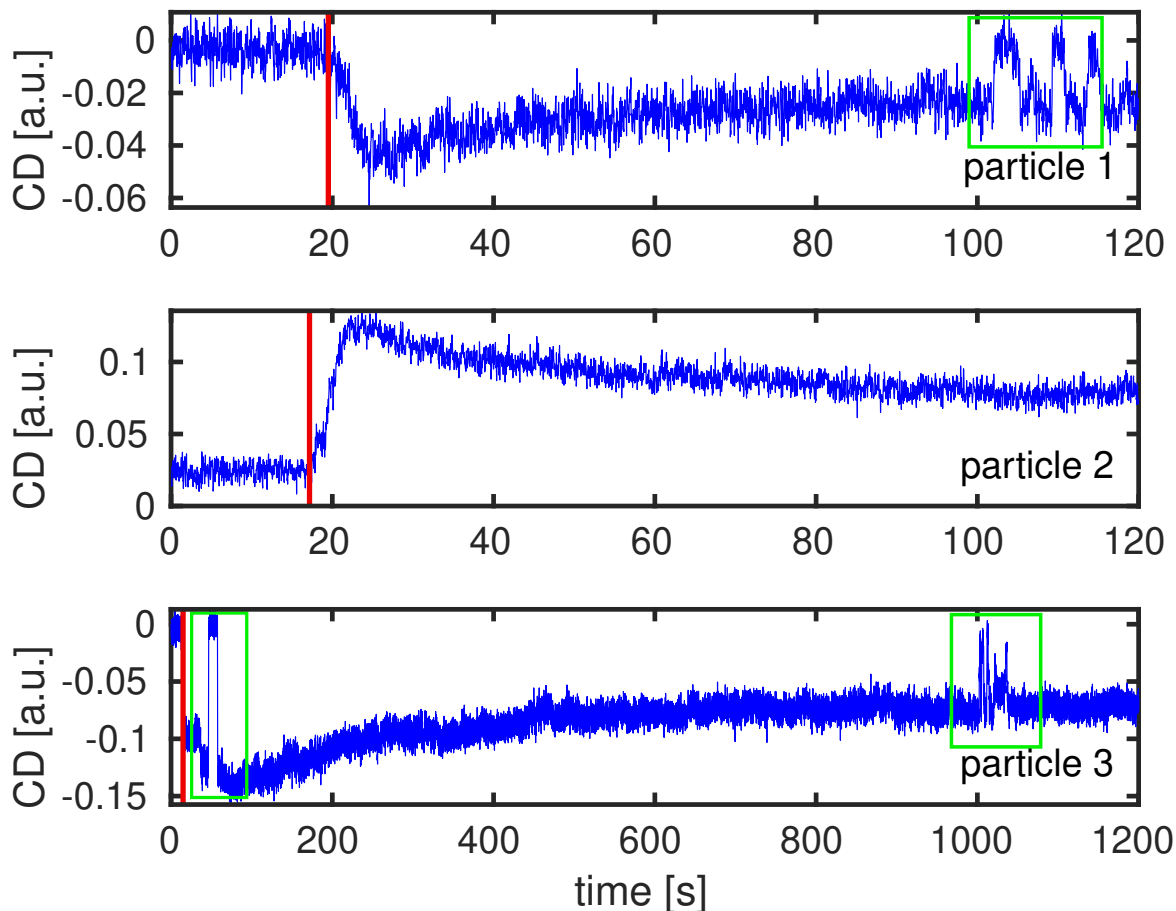


Figure S8: Time trace of CD measurements of three different 100 nm gold nanoparticles at high heating laser power indicating reshaping of the nanoparticles. At the beginning of each timetrace, the laser power is kept very low and after about 20 seconds, the laser power is slowly raised to the highest laser power. The highest laser power is about 30 mW, 30 mW and 40 mW for the first, second and third particle, respectively. The heating power (wavelength of 532 nm) is spread over an area of about $20 \mu\text{m}^2$. We use 10 mW of probe power (laser wavelength of 815 nm) in confocal. The binning time is 30 ms. The red line indicates the time when we increase the heating laser power and green boxes indicate where we did manual refocusing to check that the decrease in signal is indeed due to the reshaping, but not due to any drift out of focus. The first green box in the timetrace for the third particle indicates when the heating laser was blocked for a short period of time.

Figure S8 shows time traces of three different single gold nanoparticles. We first focus on a particle with a low laser power of few mW. After a given time, indicated by the red line

in Figure S8 we slowly increase the power of the heating beam by about 30 mW to 40 mW (Koehler illumination in the area of $20 \mu\text{m}^2$). The green boxes indicate where we manually refocus to check that the decrease in signal is indeed due to the reshaping, but not due to the out-of-focus drifts. After the initial increase, which is due to the increase in heating power, we observe a gradual decrease of CD signal, which is due to reshaping. Notably the CD signal does not vanish completely even after hundreds of seconds, but stabilizes at some finite value. This is probably because of the limited heating laser power in our experiments. We think that a further increase in heating laser power could induce further reshaping and lead to weaker and weaker CD signals over longer periods of laser exposure. However, the laser power cannot be increased indefinitely, as light-induced reactions were observed to take place in such complex liquids as carvone.^{S19}

Nanofabrication of single aluminium nanorods

Aluminium nanostructures were fabricated in the Kavli Nanolab in Delft, using the following protocol in chronological order. Glass coverslips (borosilicate glass, diameter 25 mm, thickness No.1) were used as substrate. First, they were cleaned by sonication in acetone and isopropanol. The substrate was dehydrated by a bake-off at 150°C for 10 minutes and in the same equipment it underwent priming with a monolayer of HMDS (Delta RC80 apparatus) to improve the hydrophobicity of the glass surface. The samples were transferred to a spin-coater and spun with CSAR positive e-beam resist (AR-P 6200.04) at 2000 rpm followed by a soft bake for 2 min on a hotplate at 150°C . After that, the CSAR layer was covered with 11 nm of chromium through e-beam evaporation, to form a conducting layer on top of the samples and to prevent charging of the substrate during e-beam patterning. The samples were e-beam exposed with a pattern that contained arrays of aluminium rods. The dimensions of the rods were $40 \times 100 \text{ nm}$. Each array was exposed at a different dose, ranging from 70 to $200 \mu\text{C}/\text{cm}^2$. Eventually the optimal dose was chosen by means of the optical experiment. Next, the samples were stripped of chromium by submerging them in

a Cr01 TechniEtch solution for 15 s and rinsing them with DI water. The samples were first developed in pentyl acetate (1 min), then a mixture of isopropanol and methyl-isobutyl ketone (1:1) for 1 min and finally in isopropanol for 1 min. The samples were dried and subsequently residues of the developed resist were removed through a descum process by oxygen plasma etching for 30 s at 100 Watt power and 200 sccm O₂ flow. The exposed, developed and oxygen etched glass samples were then e-beam evaporated with 3 nm of Cr for adhesion, directly followed by 60 nm of aluminium. Lift-off was performed in anisole at 80 °C for at least 1 hour. Finally, the samples were rinsed of all residuals in a jet of acetone followed by rinsing in a beaker with isopropanol and drying in a N₂ stream.

References

- (S1) Spaeth, P.; Adhikari, S.; Le, L.; Jollans, T.; Pud, S.; Albrecht, W.; Bauer, T.; Calderola, M.; Kuipers, L.; Orrit, M. Circular Dichroism Measurement of Single Metal Nanoparticles Using Photothermal Imaging. *Nano Letters* **2019**, *19*, 8934–8940.
- (S2) Whittaker, E. A.; Gehrtz, M.; Bjorklund, G. C. Residual Amplitude Modulation in Laser Electro-Optic Phase Modulation. *JOSA B* **1985**, *2*, 1320–1326.
- (S3) Jellison, G.; Modine, F. Two-Modulator Generalized Ellipsometry: Theory. *Applied Optics* **1997**, *36*, 8190–8198.
- (S4) Barriel, O. A. Mueller Matrix Polarimetry of Anisotropic Chiral Media. Ph.D. thesis, Universitat de Barcelona, Barcelona, 2010.
- (S5) Arteaga, O.; Freudenthal, J.; Wang, B.; Kahr, B. Mueller Matrix Polarimetry with Four Photoelastic Modulators: Theory and Calibration. *Applied Optics* **2012**, *51*, 6805–6817.
- (S6) Gooch Housego, Pockels Cell Aligment in a Q-Switched Laser. 2017; <https://gandh.com/wp-content/uploads/2017/10/>

GH-PM-E0-Pockels-cell-alignment-for-single-pass-systems.pdf accessed
17 March 2021.

- (S7) Besteiro, L. V.; Zhang, H.; Plain, J.; Markovich, G.; Wang, Z.; Govorov, A. O. Aluminum Nanoparticles with Hot Spots for Plasmon-Induced Circular Dichroism of Chiral Molecules in the UV Spectral Interval. *Advanced Optical Materials* **2017**, *5*, 1700069.
- (S8) Govorov, A. O. Plasmon-Induced Circular Dichroism of a Chiral Molecule in the Vicinity of Metal Nanocrystals. Application to Various Geometries. *The Journal of Physical Chemistry C* **2011**, *115*, 7914–7923.
- (S9) Nesterov, M. L.; Yin, X.; Schaferling, M.; Giessen, H.; Weiss, T. The Role of Plasmon-Generated Near Fields for Enhanced Circular Dichroism Spectroscopy. *ACS Photonics* **2016**, *3*, 578–583.
- (S10) Jones, R. C. A New Calculus for the Treatment of Optical Systems. I. Description and Discussion of the Calculus. *JOSA* **1941**, *31*, 488–493.
- (S11) Hurwitz, H.; Jones, R. C. A New Calculus for the Treatment of Optical Systems. II. Proof of Three General Equivalence Theorems. *JOSA* **1941**, *31*, 493–499.
- (S12) Jones, R. C. A New Calculus for the Treatment of Optical Systems. III. The Sohncke Theory of Optical Activity. *JOSA* **1941**, *31*, 500–503.
- (S13) Jones, R. C. A New Calculus for the Treatment of Optical Systems. IV. *JOSA* **1942**, *32*, 486–493.
- (S14) Jones, R. C. A New Calculus for the Treatment of Optical System.V. A More General Formulation, and Description of Another Calculus. *JOSA* **1947**, *37*, 107–110.
- (S15) Jones, R. C. A New Calculus for the Treatment of Optical Systems. VI. Experimental Determination of the Matrix. *JOSA* **1947**, *37*, 110–112.

- (S16) Jones, R. C. A New Calculus for the Treatment of Optical Systems. VII. Properties of the N-Matrices. *JOSA* **1948**, *38*, 671–685.
- (S17) Jackson, J. D. *Classical Electrodynamics*; Wiley: New York, 1999.
- (S18) Hugonin, J.-P.; Besbes, M.; Ben-Abdallah, P. Fundamental Limits for Light Absorption and Scattering Induced by Cooperative Electromagnetic Interactions. *Physical Review B* **2015**, *91*, 180202.
- (S19) Gaiduk, A.; Ruijgrok, P. V.; Yorulmaz, M.; Orrit, M. Making Gold Nanoparticles Fluorescent for Simultaneous Absorption and Fluorescence Detection on the Single Particle Level. *Physical Chemistry Chemical Physics* **2011**, *13*, 149–153.